Editors' Suggestion

Colloidal Crystallization on Cones

Jessica H. Sun,[1] Grace H. Zhang,[2] Abigail Plummer,[3] Caroline Martin,[1] Nabila Tanjeem,[4] David R. Nelson,[1,2] and Vinothan N. Manoharan[1,2]

[1]Harvard John A. Paulson School of Engineering and Applied Sciences, Harvard University, Cambridge, Massachusetts 02138, USA

[2]Department of Physics, Harvard University, Cambridge, Massachusetts 02138, USA

[3]Department of Mechanical Engineering, Boston University, Boston, Massachusetts 02215, USA

[4]Department of Physics, California State University, Fullerton, Fullerton, California 92831, USA

(Received 1 July 2024; revised 27 September 2024; accepted 27 November 2024; published 3 January 2025)

We explore experimentally how a conical surface frustrates the growth of colloidal crystals. Whereas crystals on a cylinder can form perfect commensurate bands, crystals on a cone tend to form tilt grain boundaries with misorientation angles set by the conical geometry. However, at small cone angles, where the surface deviates only slightly from that of a cylinder, crystals can form commensurate bands, the widths limited by the emergence of dislocations. The dislocations allow the crystal to continue growing beyond the limiting width. We relate these effects to the gradient in circumference on a cone, a consequence of the Gaussian curvature localized at the apex.

DOI: 10.1103/PhysRevLett.134.018201

Studying the formation of crystals on curved surfaces illuminates how geometric constraints can lead to frustration and novel structures [1–4]. For example, crystals must stretch to conform to spherical or hyperbolic surfaces, owing to the nonzero Gaussian curvature. The resulting crystal morphologies and defect patterns are not found on flat surfaces, as shown in a host of studies on colloidal systems over the past two decades [5–13].

Less well studied are cones. Conical surfaces pose two interesting challenges for crystal growth. First, a cone has a point-source of positive Gaussian curvature at its apex, with zero Gaussian curvature on its sides. The integrated Gaussian curvature on any surface that includes the apex is equal to the deficit angle $2\pi - \varphi$, where $\varphi = 2\pi \sin(\beta/2)$ is the angle of an unwrapped cone (sector) and β is the full cone angle [Fig. 1(a)]. This geometrical frustration is present even if the cone is decapitated by snipping material from the apex [14]. Second, a crystal growing on the cone must eventually meet itself, or "close," when it wraps around. It is instructive to compare this situation to the simpler problem of crystallization on a cylinder. Theory and simulations [15–18], as well as experiments on a colloidal system [19], have shown that for a given circumference, crystals with specific orientations can close without defects on a cylinder. At other orientations, the crystals form linear boundaries known as "line slips" or "seams." Unlike a cylinder, a cone has a gradient in circumference as one moves away from the apex. Square or triangular crystals on a cone can therefore close without defects only at so-called "magic" cone angles and, even then, only for a specific crystal orientation. Recent theoretical and computational studies of crystals [20–22] and liquid crystals [14,23,24] on non-magic-angle cones have revealed a variety of interesting defect structures triggered by geometrical frustration.

Here we experimentally explore how colloidal particles with short-ranged attractions crystallize on a conical fiber. We aim to understand how the conical geometry affects not only the defect structure but also the growth process itself. A previous study examined atomic-scale crystals of tungsten disulfide grown on high-angle ($\beta \gtrapprox 20°$) silicon cones [25]. When crystals wrapped around these cones and closed, they formed tilt grain boundaries with misorientation angles equal to the sector angle φ. In this atomic-scale system, direct observation of the crystal lattice was difficult, and results depended on comparison between experiment and simulation. In our system, we can directly observe the crystal orientations, defects, and growth process at the single-particle level. Furthermore, we focus on cones with small cone angles ($\beta \lessapprox 10°$), and we look at crystals that form far from the apex. We can therefore examine how changing the cone angle affects the crystal growth as the surface deviates from a well-understood reference state, the cylinder ($\beta = 0°$). A previous computational study from our group [22] suggested that the growth of perfect crystals can be arrested by the elastic strain resulting from the gradient in circumference, even at small β.

We prepare a colloidal system with depletion attractions [Fig. 1(b)] and use confocal microscopy to image the crystallization of particles on conical glass fibers [Fig. 1(c)]. The particles are polystyrene spheres with diameter $d = 710$ nm at 0.1% volume fraction in an aqueous solution of 0.5 mM NaCl and 0.2 mg/ml sodium carboxymethyl cellulose, a polymer. The polymer, which has an approximate size $\delta = 90$ nm [26], induces a depletion attraction

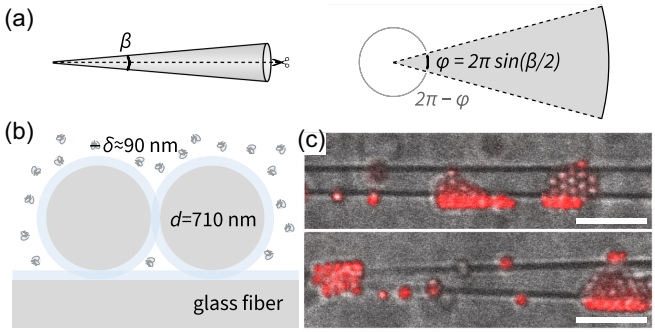

FIG. 1. (a) Left, diagram of a cone with small cone angle β. Right, diagram of the sector resulting from cutting and unwrapping the cone. The sector angle is φ. The deficit angle $2\pi - \varphi$ is equal to the integral of the Gaussian curvature enclosed by a loop around the cone apex. (b) Schematic of carboxymethyl cellulose polymers inducing depletion forces between colloidal polystyrene particles and between the particles and a glass surface. (c) Composite confocal micrograph of colloidal particles (red fluorescence channel) in the early stages of crystallizing on a cylindrical (top) and conical (bottom) glass fiber. The fibers are visible in the gray brightfield channel. The fluorescence intensity varies with the distance of the particle from the focal plane. Scale bar is 5 μm.

between the larger polystyrene spheres [27]. We choose the polymer and salt concentrations so that quasi-two-dimensional (quasi-2D) crystals form on glass substrates. To make the fibers, we stretch and taper glass capillaries with a pipette puller, varying the pulling parameters [28] to vary β between 0 and 10°.

Crystals start to form soon after the first particles adsorb onto the cone [Fig. 1(c)]. Adsorption then continues concurrently with crystal growth until, after a few hours, the crystal growth slows, likely because adsorption of particles to other surfaces in the sample chamber decreases the bulk concentration. At long times, we observe coexistence between fluid and crystalline phases on the cone [28].

At intermediate times, we can observe the closure dynamics, which appear similar for both cylinders and cones. One observed closure process involves the formation of chains that bridge the two edges of the crystal grain [Figs. 2(a) and 2(b)]. Many chains form and break before the crystal closes. We explain this observation as follows: If the grain bridged by the chain is oriented such that it could form a commensurate crystal, additional particles can easily attach to the sides of the chain and reinforce it, which closes the crystal. Otherwise, the chain remains one particle wide and is therefore susceptible to breakage. Because the grain can rotate on the surface, chains can form along different directions until the crystal closes.

However, the defect structures of crystals on cones and cylinders differ. On the cylinder, commensurate crystals can form at many orientations [18], which may explain why most crystals we observe on the cylinder are defect-free bands (Fig. S1 [28]). On the cone, crystals tend to form

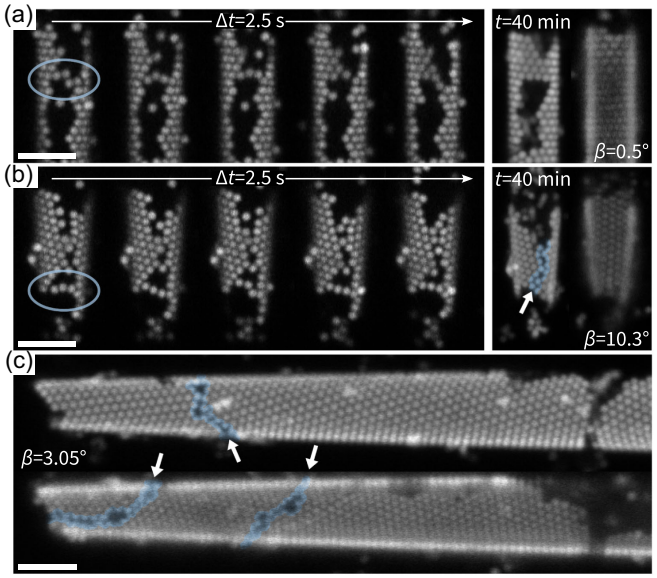

FIG. 2. Closure of crystals. (a) Time series of confocal images showing closure of a crystal on a near-cylindrical fiber ($\beta = 0.5°$). Chains of particles (circled in blue) break and reform until the crystal closes. In each closure attempt, particles and clusters rearrange and grains rotate slightly. Time between subsequent frames is 0.5 s. The crystal eventually closes to form a defect-free band, as shown by the images at right of the front and back halves of the crystal. (b) As in panel (a), but for a conical fiber ($\beta = 10.3°$). Chains also form on the cone, but the gradient in circumference leads to a seam (white arrow, blue shading). (c) Confocal projections of the front and back of a cone with a smaller cone angle ($\beta = 3.05°$) also show a seam (white arrows, blue shading; Fig. 3 shows a digital unwrapping of this cone). All scale bars are 5 μm.

visible grain boundaries when the cone angle is several degrees or more. We call these grain boundaries "seams" because they form between the edges of the same crystal Figs. 2(b) and 2(c)]. Seams arise because the gradient in circumference along the cone axis makes it impossible for the crystal to close without defects.

These results illustrate a key difference between closure on a cylinder and on a cone: when a growing grain wraps around a cone, it meets itself at a new angle. To illustrate the parallel transport associated with this phenomenon, we digitally unwrap the three-dimensional (3D) confocal images into 2D flat space to identify the grain boundary [28], as shown in Fig. S2 [28]. We then locate particles to reveal the local grain orientation with respect to a common x axis for three replicated versions of our two half-cones [Figs. 3(a) and 3(b)]. By locating particles in the flattened, 2D images instead of the 3D dataset, we can reveal the crystal orientation even when the positions of particles on the sides of the cone cannot be precisely determined.

The orientation map [28] of a crystal on a cone with $\beta = 3.05°$ reveals a single continuous grain that wraps around the surface of the cone [Fig. 3(b)]. Therefore, the

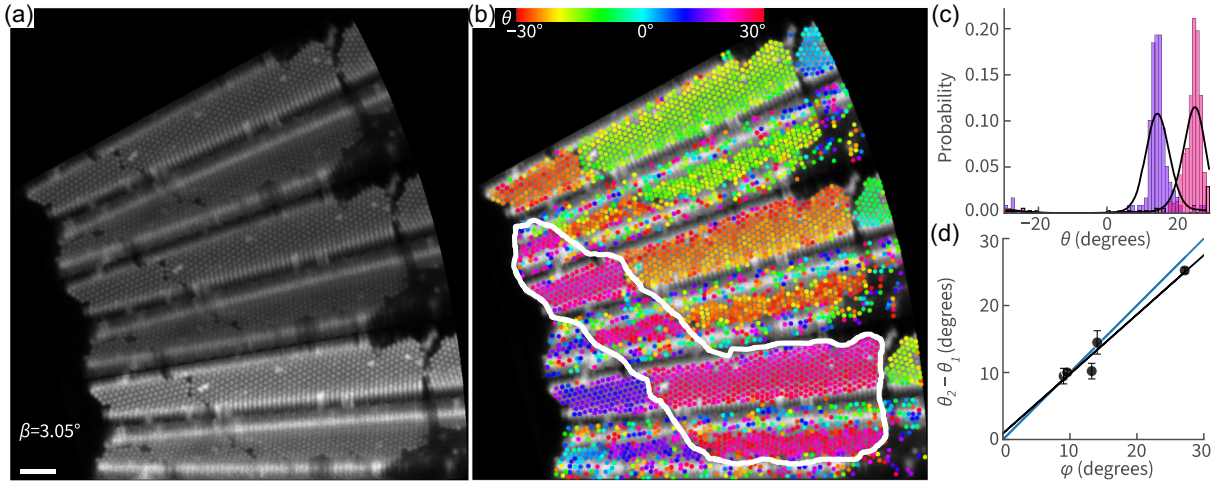

FIG. 3. Crystals on a cone are misoriented at the seam. (a) Confocal images showing two half-cones repeated three times (for visualization purposes) of the unwrapped cone from Fig. 2(b). Bright region shows the first two half-cones. Scale bar is 5 μm. (b) Color-coding particles by their local orientation relative to a global x-axis reveals that most particles are part of a single crystalline grain (white outline), as evidenced by regions of the same orientational color running across the periodic images. The outlined grain is misoriented with itself at the seam (see Fig. S3 [28] for another example). (c) Histograms and kernel density estimates (solid lines) of the local orientations of particles in the purple and pink regions in (b). The average orientations are $\theta_1 = 15.3° \pm 0.3°$ (purple region) and $\theta_2 = 25.3° \pm 0.2°$ (pink), where the uncertainties are standard errors on the means. (d) Plot of misorientation angle $\theta_2 - \theta_1$ for several crystals as a function of sector angle. A linear fit to the data (black line) agrees with the expected relationship $\theta_2 - \theta_1 = \varphi$ (blue line). For the crystal in (b), $\theta_2 - \theta_1 = 10.0° \pm 0.4°$ and $\varphi = 9.6°$.

seam that forms between the leftmost and center domains in the upper z-projection image of Fig. 2(c) is actually a tilt boundary formed between edges of the *same* grain. This boundary spirals toward the apex.

It follows by geometry that the misorientation across the seam should be equivalent to the sector angle φ of the unwrapped cone [24,25]. We calculate the misorientation from the average orientations of particles in domains adjacent to the tilt boundary and on the same side of the cone surface [Fig. 3(c)]. The measured misorientations correspond well with the sector angles [Fig. 3(d)].

Although the equivalence of the misorientation and sector angle has been found in previous experiments [25]—though indirectly as opposed to the direct measurement here—it is worth commenting on the remarkable feature it illustrates: on the cone, a global property of the surface (the cone angle) can be inferred from a local measurement (the misorientation across the grain boundary). Because the cone angle is related to the integrated Gaussian curvature around the apex, this result shows that the point source of Gaussian curvature at the apex has a long-range effect; that is, a crystal growing far from the apex, where there is no Gaussian curvature, is still subject to the strength of the point source, which forces the misorientation at closure. More generally, if the surface is not strictly a cone, the local measurement of the misorientation reveals the gradient in circumference.

To understand how this geometrical constraint might affect the growth of crystals, we examine smaller β, which allows us to probe the transition from a cylindrical to a conical geometry. At low β, we find that most crystals do not have seams like those shown in Figs. 2(b) and 2(c) over the axial length of our cones. Instead, they form crystalline bands over some length scale w_c, as shown in Fig. 4(a). We determine w_c as the largest distance between defects or voids on a crystal that has grown for at least 70 min and up to 2 h [28]. We then plot the measured w_c as a function of β [Fig. 4(b)]. For a given small range of β, there is a distribution of w_c, likely because the measured crystal width can be obscured by vacancies [28].

However, if we focus only on the largest values of w_c for each β, we find that the maximum crystal size decreases with β. For near-cylindrical surfaces, the maximum w_c is nearly as large as the entire axial length of the crystal. At high β, $w_c = 0$ because seams form that run down the cone. Figures S5(a),S5(b) [28] show crystals corresponding to the largest value of w_c for selected β.

These results show that the conical geometry limits the domain size. We originally expected, based on previous results for colloidal crystals grown on spheres [11], that the crystal size would be limited by the buildup of elastic stress. On a sphere, stress arises from the Gaussian curvature; on a cone, it arises from the gradient in circumference, determined in turn by a δ function of Gaussian curvature concentrated at the apex. A model based on a continuum approximation (see Appendix of Ref. [22] for the model and Fig. S4 [28] for a growth scenario in which this model would apply) predicts that the maximum width of a crystal grown on a cone should scale as $1/\beta$. Indeed, we find that the maximum w_c values can be fit to $w_c \sim 1/\beta$ [28], as shown in Fig. 4(b). However, if we estimate the Young's

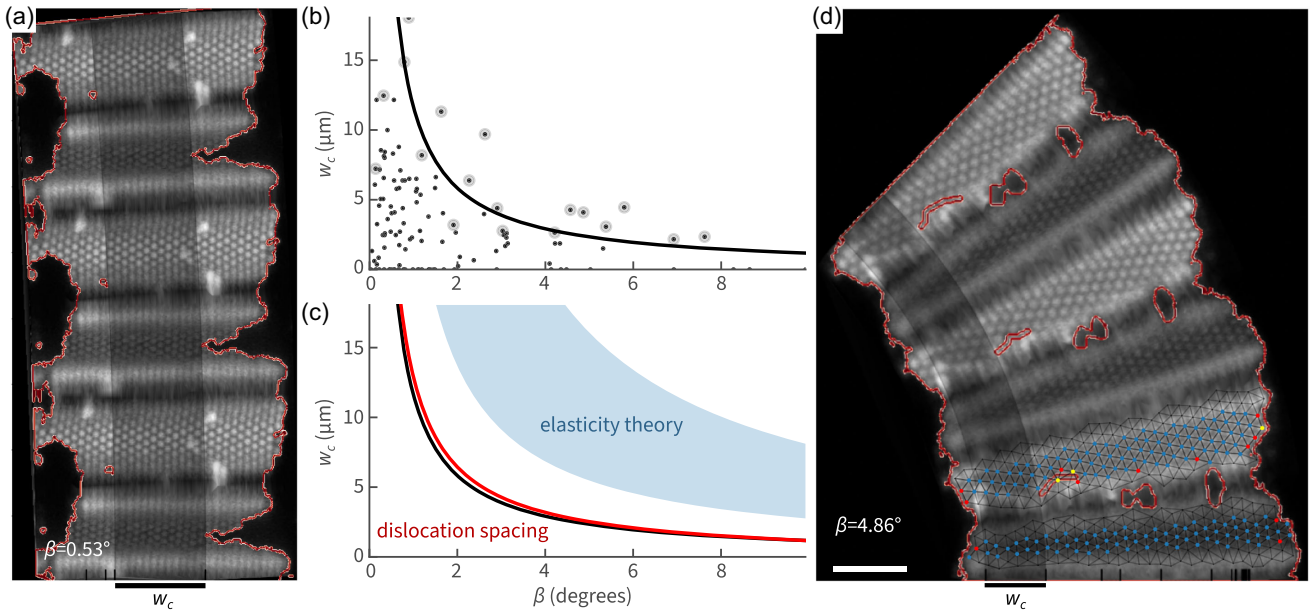

FIG. 4. The crystalline domain size is limited by the conical geometry. (a) Unwrapped images [28] of a crystal grown on a low-angle cone with $\beta = 0.53°$ ($\varphi = 1.67°$), showing that crystals form a defect-free band (dark gray region) of width $w_c = 8.31$ μm. Red borders indicate the boundaries of the crystal [28]. (b) Plot of measured w_c for 126 crystals grown on cones with $\beta = 0°$ to 9.9° ($\varphi = 0°$ to 31.2°) and diameters 3 to 9 μm. We measure w_c after allowing grains to grow and anneal for at least 70 min. Black curve shows a fit of $w_c \sim 1/\beta$ to the maximum w_c (highlighted points) at each β. (c) Plot showing the $1/\beta$ fit (black curve) and the theoretical dislocation spacing (red curve). The blue region indicates the range of maximum values of w_c if elastic strain were to limit the width. (d) Representative unwrapped image of a crystal on a cone with $\beta = 4.86°$ ($\varphi = 15.28°$) showing a dislocation. A Delaunay triangulation is overlaid on the lowest two half-cones with sixfold-coordinated particle centers in blue, fivefold in red, and sevenfold in yellow. There are unfilled cells at the half-cone boundaries because lensing distortions make it difficult to locate particles on the sides of the cones. Scale bar 5 μm.

modulus of the crystal from measurements of the pair interaction [28], we find that the continuum model predicts limiting values of w_c that do not match the data [Fig. 4(c)]. Furthermore, the Young's modulus that we estimate by assuming that the continuum model is correct does not agree with the measured modulus [28].

Instead, we find that the width of a crystal on a low-angle cone is limited by the formation of dislocations. As shown in Fig. 4(c), the fit to the experimental data closely matches [28] the expected dislocation spacing for a tilt boundary as a function of cone angle [32],

$$D = \frac{b}{\tan\varphi} = \frac{b}{\tan\left[2\pi \sin(\beta/2)\right]}, \tag{1}$$

where b is the magnitude of the dislocation Burgers vector (here, equal to the lattice constant of the crystal). For small angles, $D \sim 1/\beta$. This equation has a simple geometrical interpretation: D is the distance over which the circumference increases by a particle diameter (Fig. S6 [28]). We show a representative image of a crystal limited by dislocations in Fig. 4(d).

The formation of a dislocation releases strain such that the crystal can continue to grow axially. In systems with very short-ranged attractions, dislocations do not form because they have a prohibitively high core energy. Our system has a relatively long-ranged depletion interaction compared to previous systems [11,19], which should result in a lower dislocation core energy. The resulting dislocations screen the far-field stresses, thereby preempting the arrest mechanism predicted by the continuum elastic model. Similar types of dislocation-mediated strain reduction have been studied in twisted filament bundles [33,34] and crystalline caps [35].

Taken together, our results suggest how crystals on cones grow and close despite the geometrical frustration. Crystals initially nucleate and grow until they become large enough that their edges nearly touch. At this point, processes such as chain formation can lead to closure. On a low-angle cone, closure (likely followed by local rearrangement of particles) leads to an initially commensurate and defect-free crystalline band. As this band grows axially, it accumulates elastic strain until a dislocation forms. The crystal can then continue to grow. At larger cone angles (more than a few degrees), the larger misorientation between the edges of the crystal makes it more difficult for the crystal to close into a defect-free band. Instead, it forms a seam, or equivalently a tilt grain boundary with an angle equal to the sector angle. We note that a linear array of dislocations, with Burgers vectors perpendicular to the line, is equivalent to a grain boundary [32], which connects the two points of view.

Our findings show that a cone can geometrically frustrate crystal growth even at very low cone angles, where the dislocation spacing is large but still finite. The tapered geometry of low-angle cones is common to optical sensors [36] and electrochemical probes [37] that are immersed in biological environments, where depletion interactions can manifest. The frustration we have observed may have consequences for self-assembly in such systems. More generally, we expect that small deviations of the cone angle from *any* commensurate reference state—whether a cylinder or a magic-angle cone—will likely result in the formation of dislocations, even when a more obvious seam does not form. This concept may underlie the structural selectivity of systems that self-assemble (in the absence of a solid template) into defectless conical or cylindrical structures, such as mature HIV-1 capsids [38] or graphitic nanocones [39].

Finally, one might use the conical geometry to impose an orientation field on a colloidal crystal, so as to study the effects of misorientation on grain coarsening. Previous studies done on patterned flat surfaces [40,41] showed that crystals coarsen to remove the misorientation through grain rotation or grain splitting. On a cone, the misorientation of a crystal is prescribed, which could affect the resulting coarsening dynamics.

Acknowledgments—We thank Lara Braverman for insightful conversations. This research was primarily supported by the National Science Foundation through the Harvard University Materials Research Science and Engineering Center under Grant No. DMR-2011754. Additional support was provided by the National Science Foundation Graduate Research Fellowship Program under Grants No. DGE-2140743 and No. DGE-1745303.

Data availability—Data for the experiments are openly available on the Harvard Dataverse [42]. Code for the analysis is available under the GNU General Public License v3 [43].

[1] D. R. Nelson, Order, frustration, and defects in liquids and glasses, Phys. Rev. B **28**, 5515 (1983).
[2] G. M. Grason, Perspective: Geometrically frustrated assemblies, J. Chem. Phys. **145**, 110901 (2016).
[3] M. F. Hagan and G. M. Grason, Equilibrium mechanisms of self-limiting assembly, Rev. Mod. Phys. **93**, 025008 (2021).
[4] F. C. Meldrum and C. O'Shaughnessy, Crystallization in confinement, Adv. Mater. **32**, 2001068 (2020).
[5] A. R. Bausch, M. J. Bowick, A. Cacciuto, A. D. Dinsmore, M. F. Hsu, D. R. Nelson, M. G. Nikolaides, A. Travesset, and D. A. Weitz, Grain boundary scars and spherical crystallography, Science **299**, 1716 (2003).
[6] P. Lipowsky, M. J. Bowick, J. H. Meinke, D. R. Nelson, and A. R. Bausch, Direct visualization of dislocation dynamics in grain-boundary scars, Nat. Mater. **4**, 407 (2005).
[7] V. Vitelli, J. B. Lucks, and D. R. Nelson, Crystallography on curved surfaces, Proc. Natl. Acad. Sci. U.S.A. **103**, 12323 (2006).
[8] M. Bowick, H. Shin, and A. Travesset, Dynamics and instabilities of defects in two-dimensional crystals on curved backgrounds, Phys. Rev. E **75**, 021404 (2007).
[9] W. T. M. Irvine, V. Vitelli, and P. M. Chaikin, Pleats in crystals on curved surfaces, Nature (London) **468**, 947 (2010).
[10] W. T. M. Irvine, M. J. Bowick, and P. M. Chaikin, Fractionalization of interstitials in curved colloidal crystals, Nat. Mater. **11**, 948 (2012).
[11] G. Meng, J. Paulose, D. R. Nelson, and V. N. Manoharan, Elastic instability of a crystal growing on a curved surface, Science **343**, 634 (2014).
[12] R. E. Guerra, C. P. Kelleher, A. D. Hollingsworth, and P. M. Chaikin, Freezing on a sphere, Nature (London) **554**, 346 (2018).
[13] N. Singh, A. K. Sood, and R. Ganapathy, Observation of two-step melting on a sphere, Proc. Natl. Acad. Sci. U.S.A. **119**, e2206470119 (2022).
[14] F. Vafa, G. H. Zhang, and D. R. Nelson, Defect absorption and emission for p-atic liquid crystals on cones, Phys. Rev. E **106**, 024704 (2022).
[15] G. T. Pickett, M. Gross, and H. Okuyama, Spontaneous chirality in simple systems, Phys. Rev. Lett. **85**, 3652 (2000).
[16] A. Mughal and D. Weaire, Theory of cylindrical dense packings of disks, Phys. Rev. E **89**, 042307 (2014).
[17] A. Mughal and D. Weaire, Phyllotaxis, disk packing, and Fibonacci numbers, Phys. Rev. E **95**, 022401 (2017).
[18] D. A. Wood, C. D. Santangelo, and A. D. Dinsmore, Self-assembly on a cylinder: A model system for understanding the constraint of commensurability, Soft Matter **9**, 10016 (2013).
[19] N. Tanjeem, W. H. Wilkin, D. A. Beller, C. H. Rycroft, and V. N. Manoharan, Geometrical frustration and defect formation in growth of colloidal nanoparticle crystals on a cylinder: Implications for assembly of chiral nanomaterials, ACS Appl. Nano Mater. **4**, 10682 (2021).
[20] A. Finlay Gerrand, Colloidal crystals on conical surfaces, Ph.D. thesis, Durham University, 2021.
[21] M. A. Miller, J. O. Law, A. Finlay Gerrand, and H. Kusumaatmaja, Chapter 7—Colloidal clusters on curved surfaces, in *Frontiers of Nanoscience* (Elsevier, New York, 2022), Vol. 21, pp. 129–150.
[22] J. H. Sun, A. Plummer, G. H. Zhang, D. R. Nelson, and V. N. Manoharan, Geometric frustration of hard-disk packings on cones, Phys. Rev. E **108**, 054608 (2023).
[23] R. A. Mosna, D. A. Beller, and R. D. Kamien, Breaking the rules for topological defects: Smectic order on conical substrates, Phys. Rev. E **86**, 011707 (2012).
[24] G. H. Zhang and D. R. Nelson, Fractional defect charges in liquid crystals with p-fold rotational symmetry on cones, Phys. Rev. E **105**, 054703 (2022).
[25] H. Yu, N. Gupta, Z. Hu, K. Wang, B. R. Srijanto, K. Xiao, D. B. Geohegan, and B. I. Yakobson, Tilt grain boundary topology induced by substrate topography, ACS Nano **11**, 8612 (2017).

[26] C. W. Hoogendam, A. de Keizer, M. A. Cohen Stuart, B. H. Bijsterbosch, J. A. M. Smit, J. A. P. P. van Dijk, P. M. van der Horst, and J. G. Batelaan, Persistence length of carboxymethyl cellulose as evaluated from size exclusion chromatography and potentiometric titrations, Macromolecules **31**, 6297 (1998).

[27] R. Ganapathy, M. R. Buckley, S. J. Gerbode, and I. Cohen, Direct measurements of island growth and step-edge barriers in colloidal epitaxy, Science **327**, 445 (2010).

[28] See Supplemental Material at http://link.aps.org/supplemental/10.1103/PhysRevLett.134.018201 for full description of methods, which includes Refs. [29–31].

[29] Y. Han, N. Y. Ha, A. M. Alsayed, and A. G. Yodh, Melting of two-dimensional tunable-diameter colloidal crystals, Phys. Rev. E **77**, 041406 (2008).

[30] B. I. Halperin and D. R. Nelson, Theory of two-dimensional melting, Phys. Rev. Lett. **41**, 121 (1978).

[31] C. Martin, Precision measurements of colloidal dynamics with holographic microscopy, Ph.D. thesis, Harvard University, 2024, https://nrs.harvard.edu/URN-3:HUL.INSTREPOS:37378922.

[32] P. M. Anderson, J. P. Hirth, and J. Lothe, *Theory of Dislocations* (Cambridge University Press, New York, NY, 2017).

[33] G. M. Grason, Defects in crystalline packings of twisted filament bundles. I. Continuum theory of disclinations, Phys. Rev. E **85**, 031603 (2012).

[34] G. M. Grason, Chiral and achiral mechanisms of self-limiting assembly of twisted bundles, Soft Matter **16**, 1102 (2020).

[35] S. Li, R. Zandi, A. Travesset, and G. M. Grason, Ground states of crystalline caps: Generalized jellium on curved space, Phys. Rev. Lett. **123**, 145501 (2019).

[36] M. Pisanello, F. Pisano, L. Sileo, E. Maglie, E. Bellistri, B. Spagnolo, G. Mandelbaum, B. L. Sabatini, M. De Vittorio, and F. Pisanello, Tailoring light delivery for optogenetics by modal demultiplexing in tapered optical fibers, Sci. Rep. **8**, 4467 (2018).

[37] D. Perry, D. Momotenko, R. A. Lazenby, M. Kang, and P. R. Unwin, Characterization of nanopipettes, Anal. Chem. **88**, 5523 (2016).

[38] B. K. Ganser, S. Li, V. Y. Klishko, J. T. Finch, and W. I. Sundquist, Assembly and analysis of conical models for the HIV-1 core, Science **283**, 80 (1999).

[39] A. Krishnan, E. Dujardin, M. M. J. Treacy, J. Hugdahl, S. Lynum, and T. W. Ebbesen, Graphitic cones and the nucleation of curved carbon surfaces, Nature (London) **388**, 451 (1997).

[40] A. R. Barth, M. H. Martinez, C. E. Payne, C. G. Couto, I. J. Quintas, I. Soncharoen, N. M. Brown, E. J. Weissler, and S. J. Gerbode, Grain splitting is a mechanism for grain coarsening in colloidal polycrystals, Phys. Rev. E **104**, L052601 (2021).

[41] L. J. Moore, R. D. Dear, M. D. Summers, R. P. A. Dullens, and G. A. D. Ritchie, Direct observation of grain rotation-induced grain coalescence in two-dimensional colloidal crystals, Nano Lett. **10**, 4266 (2010).

[42] J. Sun, G. H. Zhang, A. Plummer, C. Martin, N. Tanjeem, D. R. Nelson, and V. Manoharan, Data for Colloidal crystallization on cones, Harvard Dataverse, V1 (2024), 10.7910/DVN/QAEIUV.

[43] J. H. Sun, G. H. Zhang, A. Plummer, C. Martin, V. N. Manoharan, GitHub:colloids-on-cones-code, revision number 05a0c5a (2024), https://github.com/manoharan-lab/colloids-on-cones-code.